J Nanostruct 17(1): 217-224, Winter 2027

RESEARCH PAPER

Green Synthesis of Zirconium Oxide (ZrO_2) Nanoparticles Using Mentha Leaf Extract Structural, Morphological and Antibacterial Evaluation

Zainab Hussein Mutar [1], *Dalia Yousif Salahaddin* [2], *Raheem H. Rhaif* [3]*

[1] *Ministry of Education General Directorate of Education of Babylon Wadi_Al Rafidain Boys School, Iraq*

[2] *Ministry of Education General Directorate of Education in Kirkuk, Al-Baydaa Preparatory School for Girls, Iraq*

[3] *Department of Physics, College of Science, University of Sumer, Rifai, Iraq*

ARTICLE INFO

Article History:
Received 24 August 2026
Accepted 19 October 2026
Published 01 January 2027

Keywords:
Antibacterial Activity
Green Synthesis
Mentha (mint) Extract
Zirconium Oxide Nanoparticles

ABSTRACT

Zirconium oxide nanoparticles (ZrO_2 NPs) were synthesized by a green, plant-mediated procedure, using an aqueous extract of the fresh leaves of the mint herb (*Mentha spicata*), as the reducing/capping agent and zirconium nitrate as the metal precursor. The pH of the reaction mixture was adjusted to ~9 by adding sodium hydroxide and the precipitate washed, dried at 80 °C and then calcined at 600 ° C for 2 h. The XRD data showed that the sample was formed as a single cubic ZrO_2 phase (JCPDS Card No. 96-152-1754) with the strongest reflections at $2\theta = 30.290°$ (indexed as (111)), 50.511° (indexed as (202)) and 60.044° (indexed as (311)). The Debye–Scherrer relation was used to calculate the average crystallite size, which was found to be 15.91 nm. The quasi-spherical particle morphology with mild agglomeration was observed in the sub-100 nm size range using FE-SEM micrographs, and the presence of organic residues was not observed using EDX elemental fractions (65.4 wt % Zr and 34.6 wt % O). The antibacterial activity was evaluated by the agar-well diffusion method against *Staphylococcus aureus* (*S. aureus*, Gram-positive) and *Escherichia coli* (*E. coli*, Gram-negative) at both precursor concentrations (0.5 and 1.0 M) calcined at 600 °C and pH 9. The inhibition zones of *S. aureus* and *E. coli* were 25 mm and 27 mm at 1.0 M, respectively, where the biocidal effect was clearly dose-dependent and there was a measurable sensitivity advantage for the Gram-positive strain. Overall, the results indicated that mint-extract mediated synthesis is an easy and eco-friendly method for producing robust ZrO_2 nanoparticles with potential biomedical applications.

How to cite this article
Hussein Mutar Z., Yousif Salahaddin D., Rhaif R. Green Synthesis of Zirconium Oxide (ZrO_2) Nanoparticles Using Mentha Leaf Extract Structural, Morphological and Antibacterial Evaluation. J Nanostruct, 2027; 17(1):217-224. DOI: 10.22052/JNS.2027.01.020

INTRODUCTION

Metal-oxide nanostructures continue to attract sustained interest in catalytic, optical and biological behaviors because of their high surface-to-volume ratio, tunable defect chemistry and rich surface acidity. Among them, zirconium dioxide (ZrO_2), sometimes simply called zirconia, occupies a particular place. The material is hard, chemically inert, thermally robust (melting point ≈ 2710 °C) and biocompatible, which is why it has long

* *Corresponding Author Email: rheemhussien@uos.edu.iq*

This work is licensed under the Creative Commons Attribution 4.0 International License.
To view a copy of this license, visit http://creativecommons.org/licenses/by/4.0/.

been used in dental restorations, thermal-barrier coatings, oxygen sensors and solid-oxide fuel cells [1-3]. At the nanoscale, however, the chemistry shifts: surface oxygen vacancies become more numerous, the band-gap edges sharpen, and the material develops antibacterial activity [4, 5]. Several physical and chemical routes have been used to obtain ZrO_2 nanoparticles, including sol–gel processing, hydrothermal treatment, co-precipitation, microwave-assisted synthesis and laser ablation [6-8]. While each technique has its advantages, the disadvantages are similar: high temperature, high cost of surfactant, hazardous reducing agents (such as hydrazine and $NaBH_4$), and/or organic solvents that are difficult to dispose of. However, concerns have brought the field to the "green" synthesis where the use of the conventional reagents is replaced by plant extracts. As a whole, phytochemicals like flavonoids, tannins, terpenoids and phenolic acids are not only reducing agents but also natural capping/stabilizing molecules, in which the conversion of metal to oxides takes place in water, under moderate temperature and by-products are biodegradable [9, 10].

Several plants were used for bio-mediated synthesis of ZrO_2. All of these can be given as examples: Aloe vera gel [4, 11], extract of the leaves of *Eucalyptus globulus* [12] and of *Wrightia tinctoria* [13] and *Lagerstroemia speciosa* [14]. Among less explored candidates is mint (*Mentha spicata* L.), herb whose leaves are particularly rich in rosmarinic acid, menthol, carvone and methylated flavonoids. Its phytochemical profile makes mint attractive as a multi-functional bio-template: the polyphenols reduce Zr^{4+}, the carbonyl groups bind to nascent particle surfaces, and the menthol fraction may slow grain growth during calcination. To the best of our knowledge, comparatively few systematic studies have correlated the structural, morphological and antibacterial behaviour of mint-derived ZrO_2. The present work was undertaken with three objectives. First, to demonstrate a simple aqueous green-synthesis protocol for ZrO_2 using mint-leaf extract and $Zr(NO_3)_4$ as precursor. Second, to characterize the calcined powder by X-ray diffraction (XRD), field-emission scanning electron microscopy (FE-SEM) and energy-dispersive X-ray spectroscopy (EDX) in order to verify phase, morphology and chemical purity. Third, to evaluate the antibacterial response of the prepared nanopowder against one Gram-positive (*S. aureus*) and one Gram-negative (*E. coli*) bacterium, while comparing the influence of two precursor molarities (0.5 M and 1 M) on the activity.

MATERIALS AND METHODS

Chemicals and biological materials

Zirconium nitrate pentahydrate, $Zr(NO_3)_4.5H_2O$ (analytical grade, ≥ 99 %), and sodium hydroxide pellets (NaOH, ≥ 98 %) were used as received without further purification. Distilled water was used throughout experiments. Fresh mint (*Mentha spicata* L.) leaves were obtained from a local market, and the bacterial strains *S. aureus* (ATCC 25923) and *E. coli* (ATCC 25922) were supplied by the microbiology unit of the College of Science, University of Wasit.

Preparation of the mint-leaf extract

Approximately 25.0 g of fresh, undamaged mint leaves were rinsed several times with tap water and then with distilled water to remove dust and surface contaminants. The leaves were chopped into small pieces and immersed in 250 mL of distilled water held at 60 °C for 30 min under gentle magnetic stirring. The greenish extract was allowed to cool to room temperature and was filtered through Whatman No. 1 paper. The clear filtrate was kept refrigerated at 4 °C and used within 48 h.

Synthesis of ZrO_2 nanoparticles

A solution of $Zr(NO_3)_4.5H_2O$ with a concentration of 1.0 M in distilled water was prepared by dissolving the corresponding mass of the salt in 50 mL of distilled water, while a second solution of the same salt was prepared with a concentration of 0.5 M in the same way, for the study of the dependence of molarity. The precursor solution was then drop-wise added to the mint extract at 60 °C with continuous magnetic stirring, such that the ratio of extract to precursor solution was maintained at about 1:1. NaOH solution was added drop-wise after 30 min of mixing until the pH value reached 9 ± 0.2, with almost immediate appearance of a milky-white precipitate. The stirring was continued for another hour to insure complete precipitation. The slurry was placed in centrifuge tubes (4000 rpm, 10 min) and the supernatant was removed. The solid collected was washed with distilled water/ethanol and dried overnight in a hot-air oven at 80 °C. Finally,

CC BY

the dried powder was converted into a fine white powder of ZrO_2 nanoparticles by calcining it in a muffle furnace at 600 °C, for 2 h with a heating rate of about 5 °C min^{-1}. A flow chart of the overall process is given in Fig. 1.

Antibacterial assay

The biocidal activity of the calcined ZrO_2 nanopowders (0.5 M and 1.0 M batches, both pH 9, calcined at 600 °C) was assessed using the agar-well diffusion technique. Mueller–Hinton agar plates were inoculated with 0.1 mL of fresh bacterial suspension (≈ 10^6 CFU mL^{-1}) and spread uniformly with a sterile glass rod. Wells of 6 mm diameter were punched aseptically and each was filled with 50 µL of an aqueous nanoparticle suspension (50 µg mL^{-1}). The plates were incubated at 37 °C for 24 h, and the diameter of the clear zone surrounding each well was measured using a digital vernier caliper. Each test was performed in triplicate, and the mean value was reported.

Characterization techniques

The crystalline phase and crystallite size of the calcined powder were investigated using a powder X-ray diffractometer with Cu-Kα radiation (λ = 1.5406 Å) over the 2θ range 10°–80°. Surface morphology was studied with a TESCAN MIRA3 field-emission scanning electron microscope operating at 20 kV, using the in-beam secondary-electron detector. Elemental composition and elemental mapping were obtained from the EDX detector coupled to the same instrument. The antibacterial behavior was tested by the agar-well



Fig. 1. Schematic of ZrO_2 preparation procedure.

CC BY

diffusion method.

RESULTS AND DISCUSSION

XRD analysis

The XRD pattern of the ZrO_2 powder calcined at 600 °C is shown in Fig. 2. The diffractogram displays a set of sharp, well-defined Bragg peaks superimposed on a low and almost flat background, which indicates that the prepared powder is reasonably crystalline despite the moderate calcination temperature. All the reflections could be indexed to the cubic phase of ZrO_2, in good agreement with JCPDS Card No. 96-152-1754. No additional peaks belonging to monoclinic or tetragonal ZrO_2, to $ZrO_2 \cdot xH_2O$ or to carbonaceous residues from the mint extract were observed, suggesting that calcination at 600 °C was sufficient to drive off the organic capping layer while stabilizing the cubic polymorph. Although the cubic phase of zirconia is normally unstable below ~2370 °C, several authors have shown that nanocrystalline c-ZrO_2 can persist at room temperature when the crystallite size is below a critical limit (≈30 nm) [15, 16]. The present results fall comfortably within this size window. The three strongest reflections were located at 2θ = 30.290°, 50.511° and 60.044°, corresponding to the (111), (202) and (311) planes, respectively. The experimentally measured d-spacings (2.948, 1.805 and 1.539 Å) match the standard values (2.938, 1.799 and 1.534 Å) within ≤ 0.4 %, which lies within the resolution limit of the diffractometer and confirms the structural assignment.

The average crystallite size, *D*, was estimated from the Scherrer equation:

$$D = K\lambda / (\beta \cos \theta) \quad (1)$$

where *K* (≈0.9) is the shape factor, λ is the X-ray wavelength, β is the full-width-at-half-maximum of the peak (in radians) and θ is the Bragg angle. The values obtained for the three planes were 16.53, 16.6 and 14.6 nm, giving an average crystallite size of 15.91 nm (Table 1). The slight reduction in size at higher 2θ (the (311) plane) is consistent with anisotropic growth and with the typical broadening observed for high-index reflections in nanocrystalline oxides.

FE-SEM morphology

Representative FE-SEM images recorded at different magnifications (Fig. 3) reveal that the calcined ZrO_2 powder consists of nearly spherical to

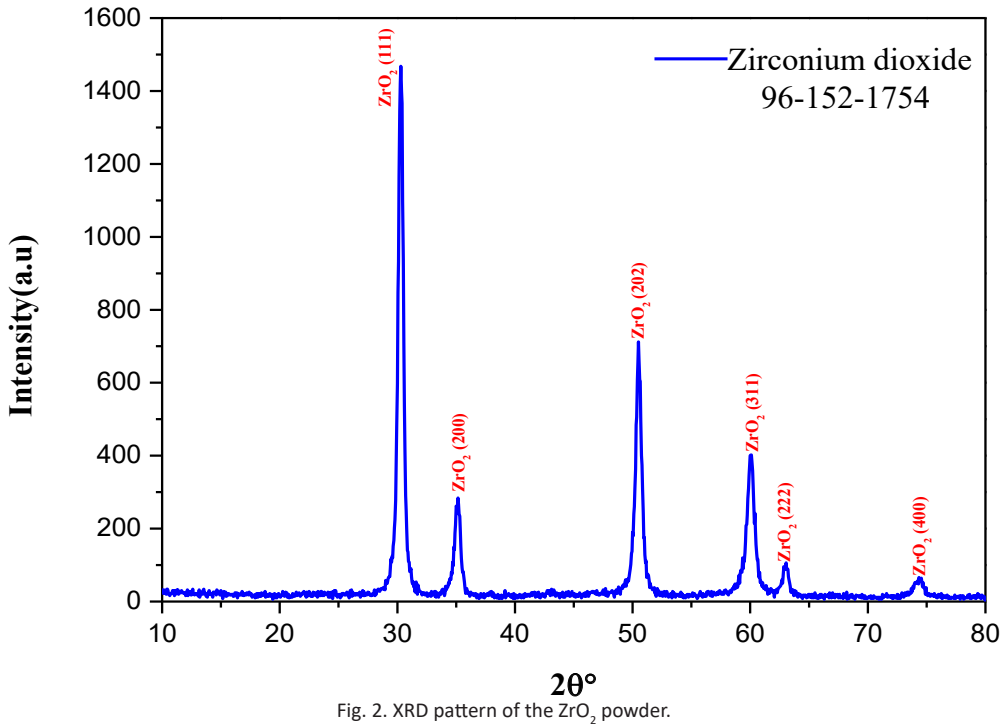


Fig. 2. XRD pattern of the ZrO_2 powder.

CC BY

quasi-spherical primary particles. Some clustering can be seen, particularly at lower magnification, where the particles tend to form loose aggregates of a few hundred nanometers. This agglomeration is not unusual for oxide nanopowders calcined at 600 °C and is generally attributed to the high surface energy of the nanocrystallites combined with the partial sintering of neck regions during heat treatment [17]. At scale of 200 nm, the individual grains become visible, and most of them lie in the 15–30 nm range, in good qualitative agreement with the XRD-derived crystallite size of ≈15.9 nm. The somewhat larger apparent grain size in SEM relative to XRD is consistent with the well-known fact that XRD reports the size of coherently diffracting domains, while SEM detects the whole particle, which may contain more than one such domain.

EDX and elemental mapping

The EDX spectrum (Fig. 4) shows two strong peaks corresponding to Zr (Kα ≈ 2.04 keV, with weaker L lines below 2 keV) and O (Kα ≈ 0.52 keV). No peaks associated with carbon, nitrogen or sodium were detected, demonstrating that the washing protocol effectively removed nitrate and sodium residues, and that calcination eliminated the organic capping layer. The quantitative output gave 65.4 wt % Zr and 34.6 wt % O (corresponding to 56.5 at % Zr and 43.5 at % O). The Zr:O atomic ratio of about 1:0.77 is below the stoichiometric value expected for ZrO_2 (1:2); this slight oxygen deficiency is characteristic of nanocrystalline ZrO_2 and is usually associated with surface oxygen vacancies, which are also responsible for the

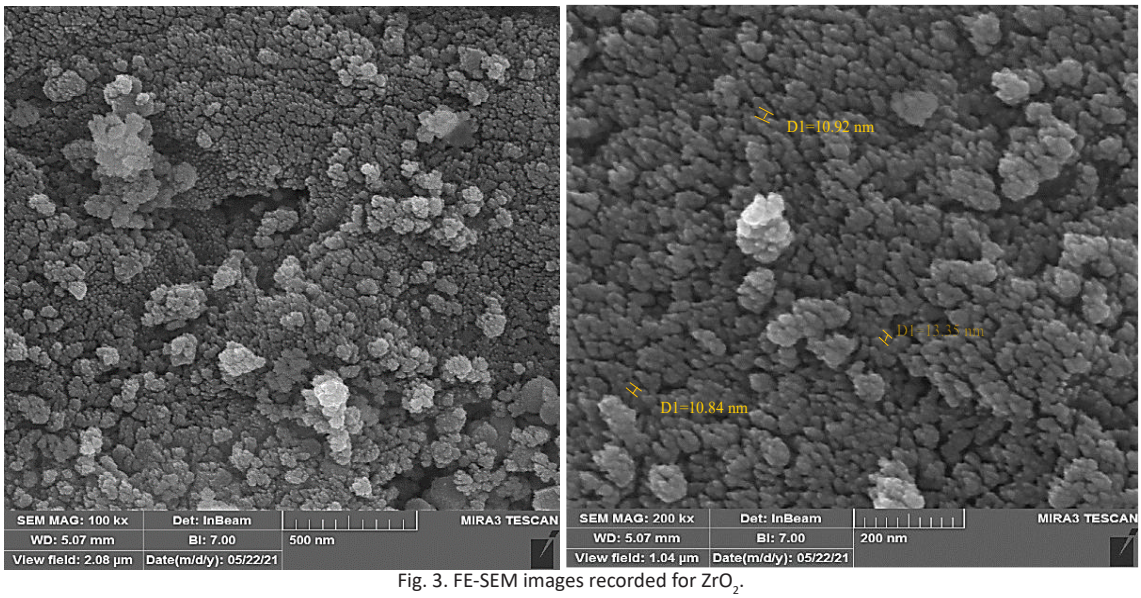


Fig. 3. FE-SEM images recorded for ZrO_2.

Table 1. XRD parameters of the green-synthesized ZrO_2 nanopowder calcined at 600 °C.

Parameter	Peak 1	Peak 2	Peak 3	Average Crystallite size
2θ (deg.)	30.290	50.511	60.044	15.91
(hkl)	(111)	(202)	(311)	
d_{hkl} exp. (Å)	2.948	1.805	1.539	
d_{hkl} std. (Å)	2.938	1.799	1.534	
Crystallite size (nm)	16.53	16.60	14.60	
Card no. (cubic phase)	96-152-1754	96-152-1754	96-152-1754	

CC BY

cubic-phase stabilization observed by XRD [18]. The EDX elemental maps confirmed a uniform spatial distribution of Zr and O over the sample area, with no segregation or localized clustering.

Antibacterial activity

The anti-bacterial effect of the green synthesized ZrO_2 nanoparticles is summarized in Table 2 and illustrated in Fig. 5. The clear, well-defined inhibition zones around the wells that had the nano powder showed both bacterial strains inhibited growth. In the case of the control wells without ZrO_2, the inhibition zone was 0 mm. These data show that the effect is concentration-dependent: that is, when the initial molarity of the precursor (the more densely packed the nanoparticles in the well) is higher, the zone of inhibition is larger, and this happens more strongly in the case of *E. coli* (Δ = 4 mm) than *S. aureus* (Δ = 1 mm). Second, *S. aureus* (Gram-positive) was systematically more sensitive than *E. coli* (Gram-negative). This pattern is consistent with several reports on metal-oxide nanoparticles [19, 20] and is normally attributed to differences in the cell-wall architecture: the thick but relatively permeable peptidoglycan layer of Gram-positive bacteria allows easier ingress of nanoparticles and reactive oxygen species, while the outer lipopolysaccharide membrane of Gram-negative bacteria functions as an additional diffusion barrier.

The biocidal mechanism of ZrO_2 nanoparticles is generally accepted to involve a combination of three pathways: (i) direct membrane disruption by sharp-edged nanoparticles and electrostatic

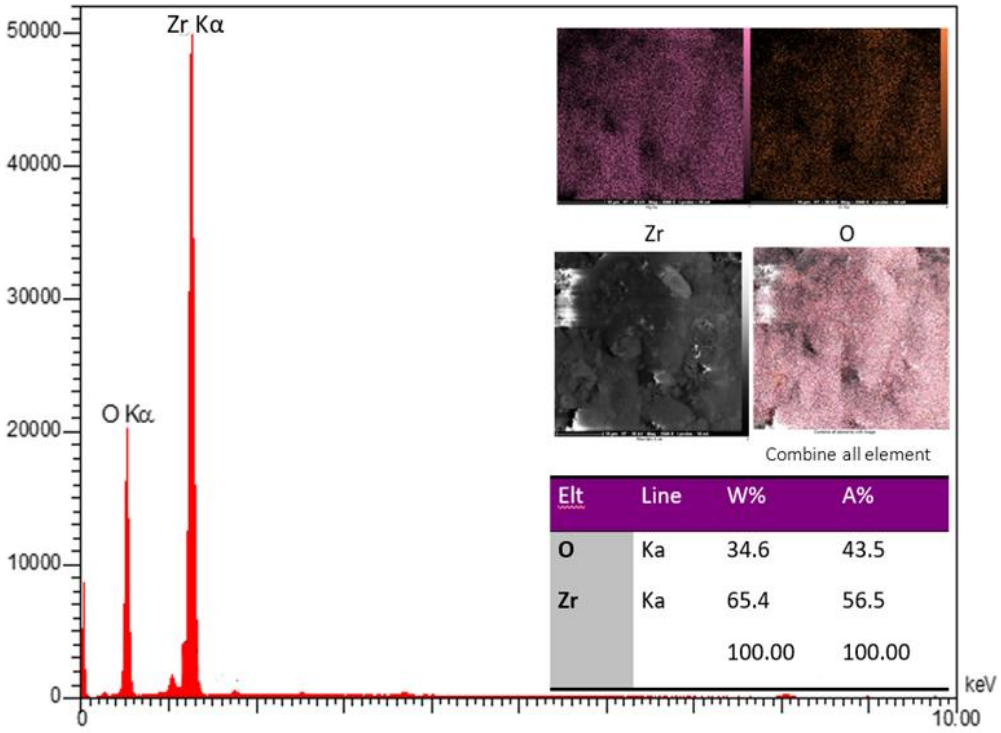


Fig. 4. EDX spectrum for ZrO_2 NPs.

Table 2. Inhibition-zone diameters (mm) of the calcined ZrO_2 nanoparticles against S. aureus and E. coli.

Bacterial strain	0.5 M, pH 9, 600 °C	1 M, pH 9, 600 °C
Staphylococcus aureus (Gram +)	26	27
Escherichia coli (Gram −)	21	25
Control (no ZrO_2)	0	0

CC BY

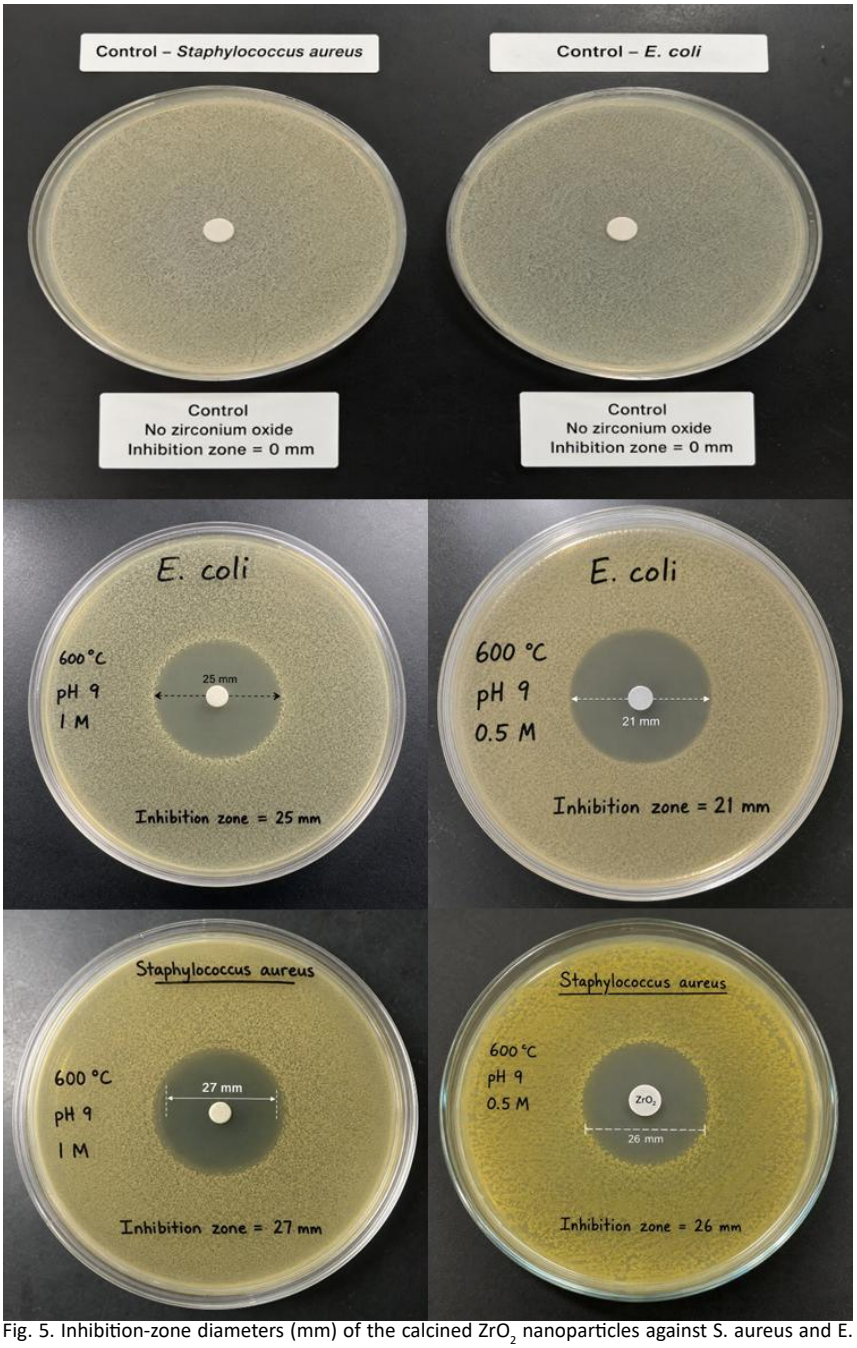


Fig. 5. Inhibition-zone diameters (mm) of the calcined ZrO_2 nanoparticles against S. aureus and E. coli.

interaction between the slightly positive nanoparticle surface and the negatively charged bacterial wall; (ii) generation of reactive oxygen species (•OH, $O_2^{\bullet-}$, H_2O_2) at oxygen-vacancy sites of the cubic lattice, which oxidize lipids, proteins and DNA; and (iii) leaching of Zr^{4+} ions, and can interfere with intracellular enzymatic processes [21, 22]. The high oxygen-vacancy density inferred from the sub-stoichiometric EDX composition supports the second pathway as a dominant contribution in the present sample.

CONCLUSION

A simple, low-cost, and environmentally

(cc) BY

benign route for ZrO_2 nanoparticles has been demonstrated using fresh mint (*Mentha spicata*) leaf extract as a multi-functional bio-template. Calcination at 600 °C produced a phase-pure cubic ZrO_2 powder with an average crystallite size of 15.91 nm, as confirmed by XRD. FE-SEM revealed quasi-spherical primary particles in the 15–30 nm range, while EDX confirmed elemental purity and a slight oxygen sub-stoichiometry consistent with the stabilization of the cubic polymorph by surface vacancies. The agar-well diffusion test showed that the nanoparticles are biologically active against both *S. aureus* and *E. coli*, with maximum inhibition zones of 27 mm and 25 mm, respectively, at 1.0 M precursor concentration. The activity is dose-dependent and stronger against the Gram-positive strain, in line with the cell-wall-permeability argument. Overall, the results indicate that mint-mediated green synthesis is a viable, scalable alternative to conventional chemical routes for the production of antibacterial ZrO_2 nanoparticles, with potential applications in wound dressings, water disinfection, and antimicrobial coatings.

CONFLICT OF INTEREST

The authors declare that there is no conflict of interests regarding the publication of this manuscript.

REFERENCES

1. Chevalier J, Gremillard L, Virkar AV, Clarke DR. The Tetragonal-Monoclinic Transformation in Zirconia: Lessons Learned and Future Trends. J Am Ceram Soc. 2009;92(9):1901-1920.
2. Garvie RC, Hannink RH, Pascoe RT. Ceramic Steel? Sintering Key Papers: Springer Netherlands; 1990. p. 253-257. http://dx.doi.org/10.1007/978-94-009-0741-6_14
3. Lughi V, Sergo V. Low temperature degradation -aging- of zirconia: A critical review of the relevant aspects in dentistry. Dent Mater. 2010;26(8):807-820.
4. Gowri S, Rajiv Gandhi R, Sundrarajan M. Structural, Optical, Antibacterial and Antifungal Properties of Zirconia Nanoparticles by Biobased Protocol. Journal of Materials Science and Technology. 2014;30(8):782-790.
5. Annu, Ali A, Ahmed S. Green Synthesis of Metal, Metal Oxide Nanoparticles, and Their Various Applications. Handbook of Ecomaterials: Springer International Publishing; 2018. p. 1-45. http://dx.doi.org/10.1007/978-3-319-48281-1_115-1
6. Tyagi B, Sidhpuria K, Shaik B, Jasra RV. Synthesis of Nanocrystalline Zirconia Using Sol–Gel and Precipitation Techniques. Industrial and Engineering Chemistry Research. 2006;45(25):8643-8650.
7. Joo J, Yu T, Kim YW, Park HM, Wu F, Zhang JZ, et al. Multigram Scale Synthesis and Characterization of Monodisperse Tetragonal Zirconia Nanocrystals. Journal of the American Chemical Society. 2003;125(21):6553-6557.
8. Hassan SMu, Siddique MT, Fakhar-e-Alam M, Atif M, Saifullah A, Marwat N, et al. Hydrothermally synthesized lanthanide-incorporated multifunctional zirconia nanoparticles: Potential candidate for multimodal imaging. Journal of King Saud University - Science. 2022;34(5):102080.
9. Jadoun S, Arif R, Jangid NK, Meena RK. Green synthesis of nanoparticles using plant extracts: a review. Environ Chem Lett. 2020;19(1):355-374.
10. Ahmed S, Ahmad M, Swami BL, Ikram S. A review on plants extract mediated synthesis of silver nanoparticles for antimicrobial applications: A green expertise. Journal of Advanced Research. 2016;7(1):17-28.
11. Alsharari SS, Alenezi MA, Al Tami MS, Soliman M. Recent advances in the Biosynthesis of Zirconium Oxide Nanoparticles and their Biological Applications. Baghdad Science Journal. 2023;20(1):0041.
12. Sadiq MU, Shah A, Haleem A, Shah SM, Shah I. Eucalyptus globulus Mediated Green Synthesis of Environmentally Benign Metal Based Nanostructures: A Review. Nanomaterials. 2023;13(13):2019.
13. Al-Zaqri N, Muthuvel A, Jothibas M, Alsalme A, Alharthi FA, Mohana V. Biosynthesis of zirconium oxide nanoparticles using Wrightia tinctoria leaf extract: Characterization, photocatalytic degradation and antibacterial activities. Inorg Chem Commun. 2021;127:108507.
14. Shashiraj KN, Hugar A, Kumar RS, Rudrappa M, Bhat MP, Almansour AI, et al. Exploring the Antimicrobial, Anticancer, and Apoptosis Inducing Ability of Biofabricated Silver Nanoparticles Using Lagerstroemia speciosa Flower Buds against the Human Osteosarcoma (MG-63) Cell Line via Flow Cytometry. Bioengineering. 2023;10(7):821.
15. Garvie RC. Stabilization of the tetragonal structure in zirconia microcrystals. The Journal of Physical Chemistry. 1978;82(2):218-224.
16. Štefanić G, Musić S. Microstructural Analysis of Boehmite Nanoparticles Prepared by Rapid Hydrolysis of Aluminum Sec-butoxide. Croat Chem Acta. 2011:481-485.
17. Aghazadeh M, Golikand AN, Ghaemi M. Synthesis, characterization, and electrochemical properties of ultrafine β-Ni(OH)$_2$ nanoparticles. Int J Hydrogen Energy. 2011;36(14):8674-8679.
18. Kalita P, Saini S, Rajput P, Jha SN, Bhattacharyya D, Ojha S, et al. Oxygen vacancy mediated cubic phase stabilization at room temperature in pure nano-crystalline zirconia films: a combined experimental and first-principles based investigation. Physical Chemistry Chemical Physics. 2019;21(40):22482-22490.
19. Adams LK, Lyon DY, Alvarez PJJ. Comparative eco-toxicity of nanoscale TiO_2, SiO_2, and ZnO water suspensions. Water Res. 2006;40(19):3527-3532.
20. Azam A, Ahmed, Oves, Khan, Habib, Memic A. Antimicrobial activity of metal oxide nanoparticles against Gram-positive and Gram-negative bacteria: a comparative study. International Journal of Nanomedicine. 2012:6003.
21. Jalal R, Goharshadi EK, Abareshi M, Moosavi M, Yousefi A, Nancarrow P. ZnO nanofluids: Green synthesis, characterization, and antibacterial activity. Materials Chemistry and Physics. 2010;121(1-2):198-201.
22. Li Y, Zhang W, Niu J, Chen Y. Mechanism of Photogenerated Reactive Oxygen Species and Correlation with the Antibacterial Properties of Engineered Metal-Oxide Nanoparticles. ACS Nano. 2012;6(6):5164-5173.

CC BY